THE GEOLOGICAL SOCIETY OF AMERICA®

Decoupling of Zr-Hf during contact metamorphic anatexis of metabasalts and timing of zircon growth, Sudbury, Canada

Taus R.C. Jørgensen[1], Douglas K. Tinkham[1], C. Michael Lesher[1], and Joseph A. Petrus[1,2]
[1]Mineral Exploration Research Centre, Harquail School of Earth Sciences and Goodman School of Mines, Laurentian University, 935 Ramsey Lake Road, Sudbury, Ontario P3E 2C6, Canada
[2]School of Earth Sciences, University of Melbourne, Corner Swanston & Elgin streets, Parkville, VIC 3010, Australia

ABSTRACT

Whole-rock Zr-Hf systematics combined with zircon petrography, geochronology, and geochemistry in partially melted mafic rocks offer new insights into Zr-Hf decoupling processes during metamorphism. Zirconium and Hf are frequently used to interpret the petrogenesis of mafic igneous rocks, but their behavior during dehydration and partial melting is still controversial. The contact aureole of the 1850 Ma Sudbury Igneous Complex (SIC, Canada) includes pyroxene hornfels facies metabasalts with systematically strong negative whole-rock Zr/Zr* (down to 0.25) and Zr/Hf (down to 29.7) anomalies. This signature only occurs in the highest grade portions of the aureole where partial melting occurred proximal to the SIC, and indicates that Zr-Hf decoupling is linked to partial melting and melt segregation. In this zone, the metabasalts contain intergranular melt with rare interstitial and poikilitic zircon grains yielding an 1850 ± 24 Ma U-Pb age, connecting zircon growth to partial melting processes. In addition, zircon texturally overgrows the peak contact metamorphic mineral assemblage and locally shows straight crystal faces in microleucosomes. This is consistent with zircon crystallizing from trapped melt and in agreement with models suggesting that metamorphic zircon does not necessarily grow during peak pressure-temperature conditions. The apparent requirement for melt to facilitate zircon growth and Zr-Hf mobility illustrates the importance of melting for understanding zircon and Zr-Hf behavior in mafic rocks. An increased understanding of whole-rock Zr-Hf decoupling combined with zircon analysis provides the opportunity of better constraining high-temperature crustal processes involving silicate melts.

By combining whole-rock Zr-Hf analyses with zircon petrography, geochemistry, and geochronology, it is possible to show that the development of Zr/Zr* and Zr/Hf anomalies in metabasalts in the SIC contact aureole are directly linked to partial melting processes. In addition, this study contradicts the assumption that metamorphic zircon grows during peak metamorphic pressure-temperature conditions, as proposed in a number of studies (Roberts and Finger, 1997; Kohn et al., 2015).

INTRODUCTION

Zr-Hf systematics are often essential to interpreting the petrogenesis of igneous and metamorphic mafic rocks, and thus important for understanding the evolution of the Earth's crust and mantle. Although there are many studies exploring the behavior of Zr-Hf during the formation and metamorphism of mafic rocks (e.g., to understand element transfer in subduction zones), the Sudbury Igneous Complex (SIC, Canada) contact aureole provides a unique setting to evaluate the processes of partial melting and zircon growth in mafic rocks and relate it to the Zr-Hf behavior resulting in Zr/Hf fractionation and Zr/Zr* anomalies.

Zirconium and Hf are thought to be largely immobile during metamorphism until partial melting occurs or until depths exceeding ~160 km are reached, where the properties of fluids and silicate melts converge to form a supercritical liquid capable of mobilizing Zr and Hf (Watson and Harrison, 1983; Rubatto and Hermann, 2003; Kessel et al., 2005). Decoupling of Zr-Hf is often negligible during igneous processes involving silicate melt, as is demonstrated by chondritic ratios in global geochemical reservoirs such as mid-oceanic ridge basalt (MORB; David et al., 2000). However, experimental data suggest that Zr is more compatible than Hf (i.e., $D_{Zr}^{\text{hydrous melt/solid}} < D_{Hf}^{\text{hydrous melt/solid}}$, where D is the partition coefficient) during subduction-related partial melting (1000 °C and 40 kbar) of average MORB (Kessel et al., 2005), resulting in higher Zr/Hf values in the restite. As such, the wide range of Zr/Hf observed in some blueschist and eclogite facies metabasalts (e.g., Sorensen et al., 1997; Zr/Hf from ~26–290 and an average of ~45 ± 6.3, 1 standard error), the remnants of subducted ocean crust, does not offer a clear picture on the processes controlling the decoupling of Zr-Hf.

Rubatto and Hermann (2003) showed that zircon, when present in subducted oceanic crust, is the dominant host for Zr (>95%) and Hf (~90%), and thus segregated fluids and melts capable of dissolving zircon should be essential to the transfer of Zr and Hf in subduction zones. However, recent Zr mass balance models suggest that melting may not be crucial for understanding zircon behavior in mafic rocks (Kohn et al., 2015).

GEOLOGICAL SETTING

The two-pyroxene hornfels metabasalts reported in this study are part of the Elsie Mountain Formation (EMF), which has a minimum age of 2452.5 ± 6.2 Ma (Ketchum et al., 2013) and occurs in the lowermost Paleoproterozoic Huronian Supergroup in the Sudbury area, Canada (Fig. 1; Fig. DR1 in the GSA Data Repository[1]). The EMF is the easternmost part of an ~200-km-long volcanic belt interpreted to represent flood basalts associated with continental rifting (Jolly et al., 1992). The EMF in the Sudbury area is composed of pillowed and massive basalt flows that form part of the footwall rock along the southern margin of the SIC (e.g., Innes, 1977; Jolly et al., 1992). The SIC is the remnant of an impact melt sheet that was initially superheated to ~1800 °C and had the geometry of a <5-km-thick magma pond with a diameter exceeding 100 km (Lightfoot,

[1]GSA Data Repository item 2018036, Appendix DR1 (zircon isotope and trace element analytical techniques and methods), Appendix DR2 (whole-rock trace element analytical techniques and methods), Figure DR1 (regional geological map showing the distribution of the Huronian metavolcanic rocks), Figure DR2 (back-scattered electron, cathodoluminescence [CL], and secondary electron images of zircon grains), Figure DR3 (CL and element maps of zircon grains), Figure DR4 (heavy rare earth element chondrite-normalized diagram for zircon analyses), Figure DR5 (mesoscopic leucosomes within the Elsie Mountain Formation [EMF] metabasalts), Table DR1 (U-Pb and trace element data for zircon in EMF metabasalts), and Table DR2 (whole-rock trace element geochemistry for EMF metabasalts), is available online at http://www.geosociety.org/datarepository/2018/ or on request from editing@geosociety.org.

GEOLOGY, February 2018; v. 46; no. 2; p. 159–162 | GSA Data Repository item 2018036 | https://doi.org/10.1130/G39590.1 | Published online 20 December 2017

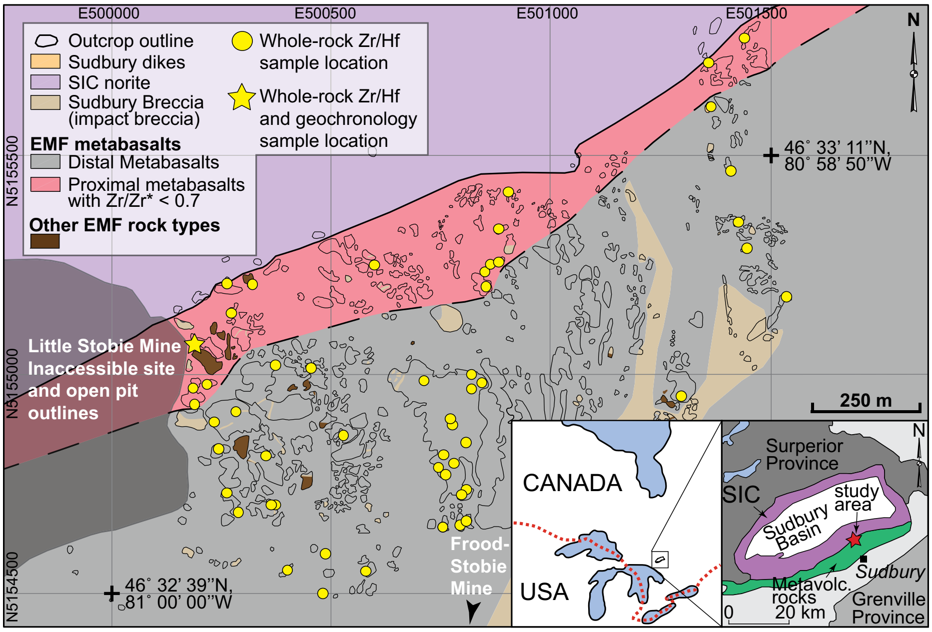

Figure 1. Geological map showing sample locations for Elsie Mountain Formation (EMF, Sudbury, Canada) metabasalts in the Sudbury Igneous Complex (SIC) contact aureole. Metabasalts with Zr/Zr* < 0.7 and zircon described in the text are confined to the proximal contact aureole (regional setting in Fig. DR1 [see footnote 1]). Metavolc.—metavolcanic.

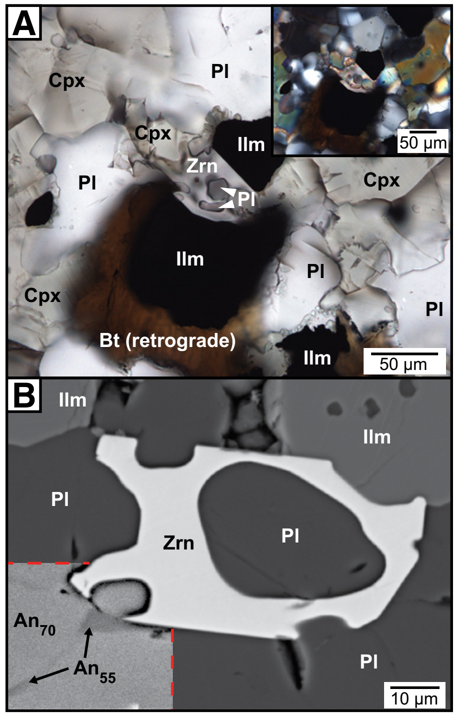

Figure 2. A: Irregular and poikilitic zircon (Zrn; R-S33) with inclusions of plagioclase (Pl) and in contact with clinopyroxene (Cpx), ilmenite (Ilm), and matrix plagioclase. Bt—biotite. Inset shows the same field of view in cross-polarized light, highlighting the granoblastic polygonal texture of the high-temperature mineral assemblage. B: Backscattered electron image with contrast in lower left corner (indicated by red dashed lines) adjusted to better show the presence of two compositionally distinct plagioclase phases (An_{55} and An_{70}; An—anorthite component of plagioclase). The low-Ca plagioclase reflects trapped partial melt in the hornfels rocks.

2016, and references therein). The dimensions and high temperature of the melt sheet resulted in extensive contact metamorphism of the underlying footwall rocks.

The metamorphic history of the EMF includes pre- and post-SIC regional events (Card, 1978; Riller, 2005). Post-impact Penokean orogenic temperatures at the Garson Mine, Sudbury, peaked at 550–590 °C and had declined to ~400 °C by 1849 ± 6 Ma (U-Pb isotope dilution–thermal ionization mass spectrometry, ID-TIMS, titanite age; Mukwakwami et al., 2014). However, parts of the contact aureole in the footwall along the southern margin of the SIC escaped metamorphic overprinting (Jørgensen, 2017). The peak contact metamorphic mineral assemblage in EMF metabasalts is plagioclase-clinopyroxene-orthopyroxene-magnetite-ilmenite (Jørgensen, 2017). Textural evidence for partial melting is provided by mesoscopic and microscopic leucosomes defined by anhedral cuspate quartz and relatively Ca-poor plagioclase networks along grain boundaries of relatively Ca-rich plagioclase and pyroxene (Jørgensen, 2017). Geochemical signatures suggestive of partial melting are recorded in EMF metabasalts in the innermost contact aureole of the SIC that are notably depleted in Th–light rare earth elements (LREEs) relative to middle (M) and heavy (H) REEs (Jørgensen, 2017) compared to the enriched signatures observed in EMF metabasalts away from the SIC and in equivalent rocks in other parts of the volcanic belt (e.g., Ketchum et al., 2013; Jørgensen, 2017). Phase equilibria modeling of an average EMF basalt composition indicates peak contact metamorphic temperatures of at least 900 °C (Jørgensen, 2017).

ZIRCON PETROGRAPHY

Two EMF metabasalt samples from within 70 m (FSTJ301) and 10 m (FSTJ098A) of the basal contact with the SIC contain <40 ppm Zr (Fig. 1). Zircon is present in trace amounts and randomly distributed in the rocks as subrounded, subhedral, equant-stubby grains, and anhedral to subhedral, poikilitic grains. Locally, the poikilitic grains form interstitial networks with apophyses of thin (1–2 µm) films forming cuspate outlines at grain contacts between other silicate and/or oxide phases (Figs. 2A and 2B; also see Fig. DR2). The grains are dominantly between 10 and 25 µm and rarely to 30–50 µm, and only one observed grain approached 100 µm in the longest dimension. They occur in association with all phases in the peak contact metamorphic assemblage and generally share contacts with more than one of these minerals. The nature of the contacts between zircon and associated phases varies, but zircon is typically subrounded against pyroxene and straight to subrounded against oxides and plagioclase. Rounded to subrounded inclusions of relatively Ca-rich plagioclase and lesser clinopyroxene in zircon are common. Locally, zircon is in contact with only plagioclase, and is locally interstitial between relatively Na-rich plagioclase (An_{55} in sample FSTJ301; An—anorthite component of plagioclase) and polygonal granoblastic Ca-rich plagioclase (An_{70} in sample FSTJ301; Fig. 2B).

Cathodoluminescence (CL) and backscattered electron (BSE) imaging of zircon reveals the local presence of sector zoning and otherwise fairly simple internal morphologies with little to no textural indication of metamictization (Fig. DR2). Shock metamorphic features reported in other Sudbury zircon (e.g., Thomson et al., 2014) are not present. Thorite, coffinite, xenotime, thortveitite, and other phases that are commonly described in hydrothermally reequilibrated zircon are not observed as inclusions in BSE, CL, or qualitative element map images (e.g., Th, Hf, Pb, and HREEs; Figs. DR2 and DR3). The qualitative element maps also show no signs of major nonstoichiometric elements (e.g., Ca and Al; Geisler et al., 2007).

U-Pb AND TRACE ELEMENT GEOCHEMISTRY

Three zircon grains from two different thin sections of sample FSTJ301 were selected for U-Pb dating and trace element analyses by laser ablation–inductively coupled plasma–mass spectrometry (LA-ICP-MS; n = 13), and 56 samples were selected for whole-rock trace element analyses by solution ICP-MS. The

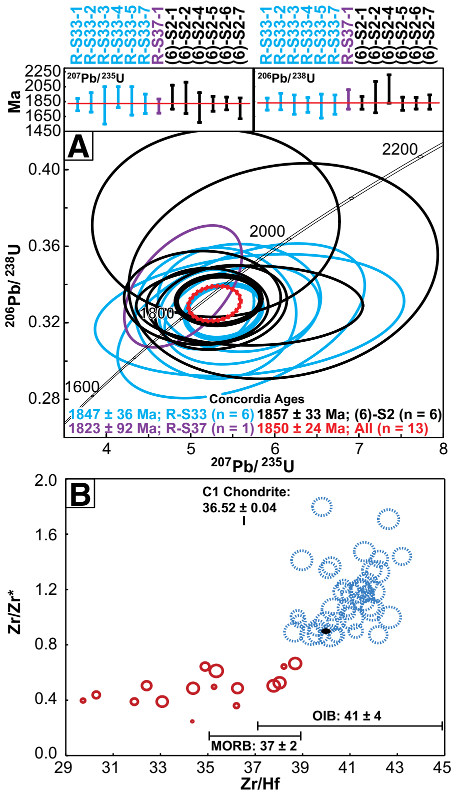

Figure 3. A: Concordia diagram showing U-Pb laser ablation–inductively coupled plasma–mass spectrometry ages of zircons in proximal Elsie Mountain Formation (EMF, Sudbury, Canada) metabasalts. Thinner error ellipses are individual analyses, whereas thicker ellipses are concordia ages for all analyses in each grain. The thick red notched error ellipse represents the concordia age calculated for all 13 analyses together and yields an age of 1850 ± 24 Ma. Insets at the top are weighted-average plots of individual analyses for both $^{207}Pb/^{235}U$ and $^{206}Pb/^{238}U$ ages. B: Whole-rock Zr/Zr* versus Zr/Hf plot showing the variations within EMF metabasalts: distal metabasalts (blue dotted circles) have higher Zr/Zr* and Zr/Hf ratios, whereas proximal two-pyroxene hornfels metabasalts (red circles) have lower Zr/Zr* and Zr/Hf ratios. Circle size is proportional to the distance from the Sudbury Igneous Complex. Mid-oceanic ridge basalt (MORB), ocean island basalt (OIB), and C1 Chondrite Zr/Hf ratios are from David et al. (2000; note that their positions do not reflect a Zr/Zr* value). Black ellipse indicates the 2σ standard deviation for analyzed standard BHVO-2 (Hawaiian Volcanic Observatory Basalt) (n = 3; Appendix DR2; see footnote 1).

analytical methods and zircon and whole-rock chemistry are presented in Appendices DR1 and DR2 and Tables DR1 and DR2. Concordia ages were calculated for each of the three grains, and yield 1847 ± 36 Ma (grain R-S33–1; n = 6), 1823 ± 92 Ma (grain R-S37; n = 1), and 1857 ± 33 Ma [grain (6)-S2; n = 6] (Fig. 3A). All 13 analyses considered together yield a concordia age of 1850 ± 24 Ma [2σ; mean square of weighted deviates $_{\text{(concordance + equivalence)}}$ = 0.68; probability $_{\text{(concordance + equivalence)}}$ = 0.88; decay-constant errors included] and are within error of the 1850 Ma SIC emplacement age (Krogh et al., 1984).

Chondrite-normalized HREE compositions of zircon from sample FSTJ301 (Fig. DR4) show a smooth decreasing trend from Lu to Gd. All analyses conform to and are bracketed by zircon trends observed in low-pressure metamorphic and magmatic zircon (Rubatto and Hermann, 2007). Titanium contents range from 3.9 to 7.0 ppm with an average of 5.2 ± 0.8 ppm (Table DR1).

Metabasalts distal to the SIC are characterized by Zr/Hf between 43.2 and 38.6 (average = 40.9 ± 2.2, 2σ) and Zr/Zr* between 1.80 and 0.87 (average = 1.15 ± 0.44, 2σ). Metabasalts proximal to the SIC are characterized by Zr/Hf between 38.7 and 29.7 (average = 34.8 ± 5.2, 2σ) and Zr/Zr* between 0.67 and 0.25 (average = 0.49 ± 0.22, 2σ; Table DR2; Fig. 3B). Zirconium* is an interpolation between Nd and Sm, and Zr/Zr* values less than unity indicate a negative anomaly (for details, see Appendix DR1; Table DR2).

DISCUSSION

Timing of Zircon Growth

Several features are consistent with zircon forming during post-peak contact metamorphic conditions: (1) the new U-Pb zircon ages reported here (Fig. 3A) overlap the Sudbury impact event; (2) there are no shock-related features (e.g., Erickson et al., 2013, Cavosie et al., 2015; Kenny et al., 2017) to suggest that the grains predate the impact; (3) the studied zircon grew around and along grain boundaries of peak contact metamorphic pyroxene, ilmenite, and relatively Ca-rich plagioclase (Fig. 2); (4) Penokean metamorphic temperatures were not high enough to form the two-pyroxene hornfels assemblage; (5) the zircon HREE profiles suggest a low-pressure metamorphic or magmatic environment (Fig. DR4); and (6) zircon locally shares a straight contact with the microleucosome and grows around the Ca-rich plagioclase in a manner similar to the microleucosomes (Fig. 2B). Taken together, we conclude that zircon formed during post-peak contact metamorphic cooling of trapped intergranular partial melts in the two-pyroxene hornfels rocks.

Decoupling of Zr-Hf

The SIC contact aureole offers new insights into the role of partial melting and melt segregation in metabasalts on the decoupling of Zr-Hf. Whole-rock Zr/Zr* and Zr/Hf systematics of the EMF metabasalts in the SIC contact aureole define two distinct but continuous populations (Fig. 3B): (1) distal (>250 m) metabasalts (dotted circles in Fig. 3B) with higher Zr/Zr* and Zr/Hf ratios, and (2) proximal (<250 m) metabasalts with lower Zr/Zr* and Zr/Hf ratios (Fig. 1). The Zr/Hf ratios of distal metabasalts are relatively consistent and similar to ocean island basalts (OIB Zr/Hf = 41 ± 4; 2σ; David et al., 2000), whereas the Zr/Hf ratios of proximal metabasalts extend across and well past the range for MORB and C1 chondrite (MORB Zr/Hf = 37 ± 2, 2σ; C1 chondrite Zr/Hf = 36.52 ± 0.04, 2σ; David et al., 2000). The higher OIB-like Zr/Hf of distal metabasalts compared to MORB can be explained by differences in mantle source composition and/or degree of mantle partial melting (David et al., 2000), but the range of Zr/Hf in proximal metabasalts exceeds the variability that can be expected to be generated within the same basaltic unit by primary magmatic processes and must therefore have been produced during post-emplacement processes. The interpretation that the whole-rock Zr-Hf systematics documented in the proximal metabasalts are related to partial melting during contact metamorphism is strongly supported by the combination of zircon petrography, chemistry, and ages (Figs. 2 and 3); the presence of mesoscopic patchy, coalescing, dike-like leucosomes within the proximal metabasalts (Fig. DR5); a concordant U-Pb LA-ICP-MS age of 1839 ± 10 Ma for zircon in the patchy leucosomes, consistent with the timing of SIC contact metamorphism (Jørgensen, 2017); and corresponding whole-rock depletion in Th-LREEs relative to MREEs and HREEs with proximity to the SIC (Jørgensen, 2017). Furthermore, these data indicate that melting reached a critical threshold (>7%; Rosenberg and Handy, 2005) in the SIC contact aureole and that melt segregation mobilized Zr and to a lesser degree Hf, producing negative Zr-Hf anomalies and fractionation of Zr/Hf during the partial melting process. The Zr/Hf ratio within the proximal zone does not vary systematically with proximity to the SIC contact, so the systematically lower Zr/Zr* but variable Zr/Hf ratios suggest both elements were mobile during high-temperature contact metamorphism, but that local variations in melt compositions (e.g., Linnen and Keppler, 2002) may have influenced the relative mobilities of Zr-Hf.

The wide range in Zr/Hf ratios in some compilations of high-pressure metabasalt (e.g., Sorensen et al., 1997) are difficult to interpret. Nonetheless, Rubatto and Hermann (2003) demonstrated that significant Zr-Hf mobilization in this environment is likely to occur only if the liquid phase is silicate melt rather than a hydrous fluid. This is consistent with observations here, i.e., the distal metabasalts all underwent variable amounts of dehydration during SIC contact metamorphism, but dehydration by itself is incapable of significantly mobilizing Zr-Hf, which also seems true for incipient melting below the melt segregation threshold. This is also supported by experimental work on average MORB at pressures below 6 GPa, where

Zr-Hf aqueous fluid-solid partition coefficients are <0.6 at 900 °C and <0.1 at 800 °C (Kessel et al., 2005). However, the generally lower Zr/Hf ratios in the proximal metabasalts suggest that the distribution coefficients for Zr and Hf between solid and liquid are reversed compared to those proposed for a higher pressure subduction setting (Kessel et al., 2005).

Zircon Behavior in Mafic Rocks

The whole-rock Zr-Hf systematics from EMF metabasalts described here required melting and melt segregation. As segregation ceased, minuscule amounts of zircon eventually formed from trapped melt films. This suggests that although the extent to which melting reactions have been observed to affect zircon consumption and growth in felsic rocks is not nearly as pronounced in mafic rocks (Kohn et al., 2015), melting is also critical for understanding zircon behavior in mafic rocks.

CONCLUSIONS

The combination of well-established methods, i.e., whole-rock Zr-Hf geochemistry, zircon petrography, geochemistry, and U-Pb geochronology, have provided the first outline of the partial melt and melt segregation zone in EMF metabasalts along the southern SIC contact aureole. The observations illustrate the importance of melting for mobilization and decoupling of Zr-Hf, and zircon behavior in mafic rocks. The results also highlight conclusions from mass-balance studies (Roberts and Finger, 1997; Kohn et al., 2015) that metamorphic zircon cannot automatically be assumed to have grown during peak-metamorphic conditions. Whole-rock Zr-Hf systematics have the potential to differentiate between dehydration and partial melting processes in metamorphosed mafic rocks. In combination with zircon analyses, such an approach might help constrain processes and conditions during subduction of oceanic crust as well as in low-pressure and high-temperature settings, e.g., basal sheeted dike-gabbro boundaries proximal to axial magma chambers (1–2 km beneath the seafloor), and in proximal metamorphic contact aureoles around igneous intrusions and impact melt sheets.

ACKNOWLEDGMENTS

Financial support was provided by grants from the Centre for Excellence in Mining Innovation, Vale Ltd., Glencore Ltd., and the Natural Sciences and Engineering Research Council of Canada (CRD 381555–09 to P. Jugo, Tinkham, and Lesher; Discovery Grant 327218–2009 to Tinkham; Discovery Grants 203171–2007 and 203171–2012 to Lesher; PDF-487902-2016 to Petrus). We are grateful to James Beard, Aaron Cavosie, and Fernando Corfu for very constructive and helpful reviews of the manuscript. Jørgensen thanks Richard Stern for discussions on how to successfully analyze the studied zircon. Field and logistical support was provided by Vale Ltd., and we thank Peter Lightfoot and Lisa Gibson of Vale for their assistance.

REFERENCES CITED

Card, K.D., 1978, Geology of the Sudbury-Manitoulin area, districts of Sudbury and Manitoulin: Ontario Geological Survey Report 166, 238 p.

Cavosie, A.J., Timms, N.E., Erickson, T.M., Hagerty, J.J., and Hörz, F., 2016, Transformations to granular zircon revealed: Twinning, reidite, and ZrO2 in shocked zircon from Meteor Crater (Arizona, USA): Geology , v. 44, p. 703–706, https://doi.org/10.1130/G38043.1.

David, K., Schiano, P., and Allègre, C.J., 2000, Assessment of the Zr/Hf fractionation in oceanic basalts and continental materials during petrogenetic processes: Earth and Planetary Science Letters, v. 178, p. 285–301, https://doi.org/10.1016/S0012-821X(00)00088-1.

Erickson, T.M., Cavosie, A.J., Moser, D.E., Barker, I.R., and Radovan, H.A., 2013, Correlating planar microstructures in shocked zircon from the Vredefort Dome at multiple scales: Crystallographic modeling, external and internal imaging, and EBSD structural analysis: American Mineralogist, v. 98, p. 53–65, https://doi.org/10.2138/am.2013.4165.

Geisler, T., Schaltegger, U., and Tomaschek, F., 2007, Re-equilibration of zircon in aqueous fluids and melts: Elements, v. 3, p. 43–50, https://doi.org/10.2113/gselements.3.1.43.

Innes, D.G., 1977, Proterozoic volcanism in the Southern Province of the Canadian Shield [M.S. thesis]: Sudbury, Canada, Laurentian University, 161 p.

Jolly, W.T., Dickin, A.P., and Wu, T., 1992, Geochemical stratigraphy of the Huronian continental volcanics at Thessalon, Ontario: Contributions of two-stage crustal fusion: Contributions to Mineralogy and Petrology, v. 110, p. 411–428, https://doi.org/10.1007/BF00344078.

Jørgensen, T.R.C., 2017, Evolution of the Sudbury Igneous Complex southern metamorphic aureole and controls on anatexis [Ph.D. thesis]: Sudbury, Canada, Laurentian University, 327 p.

Kenny G.G., Morales, L.F., Whitehouse, M.J., Petrus, J. A., and Kamber, B. S., 2017, The formation of large neoblasts in shocked zircon and their utility in dating impacts: Geology, v. 45, p. 1003–1006, https://doi.org/10.1130/G39328.1

Kessel, R., Schmidt, M.W., Ulmer, P., and Pettke, T., 2005, Trace element signature of subduction-zone fluids, melts and supercritical liquids at 120–180 km depth: Nature, v. 437, p. 724–727, https://doi.org/10.1038/nature03971.

Ketchum, K.Y., Heaman, L.M., Bennett, G., and Hughes, D.J., 2013, Age, petrogenesis and tectonic setting of the Thessalon volcanic rocks, Huronian Supergroup, Canada: Precambrian Research, v. 233, p. 144–172, https://doi.org/10.1016/j.precamres.2013.04.009.

Kohn, M.J., Corrie, S.L., and Markley, C., 2015, The fall and rise of metamorphic zircon: American Mineralogist, v. 100, p. 897–908, https://doi.org/10.2138/am-2015-5064.

Krogh, T.E., Davis, D.W., and Corfu, F., 1984, Precise U-Pb zircon and baddeleyite ages for the Sudbury area, *in* Pye, E.G., et al., eds., The geology and ore deposits of the Sudbury structure: Ontario Geological Survey Special Volume 1, p. 431–446.

Lightfoot, P.C., 2016, Nickel sulfide ores and impact melts: Origin of the Sudbury Igneous Complex: Netherlands, Elsevier, 680 p.

Linnen, R.L., and Keppler, H., 2002, Melt composition control of Zr/Hf fractionation in magmatic processes: Geochimica et Cosmochimica Acta, v. 66, p. 3293–3301, https://doi.org/10.1016/S0016-7037(02)00924-9.

Mukwakwami, J., Lafrance, B., Lesher, C.M., Tinkham, D., Rayner, N., and Ames, D.E., 2014, Fabrics and textures of deformed and metamorphosed Ni-Cu-PGE sulfide ores at Garson Mine and their implications for sulfide mobilization processes: Mineralium Deposita, v. 49, p. 175–198, https://doi.org/10.1007/s00126-013-0479-y.

Riller, U., 2005, Structural characteristics of the Sudbury impact structure, Canada: Impact-induced versus orogenic deformation—A review: Meteoritics & Planetary Science, v. 40, p. 1723–1740, https://doi.org/10.1111/j.1945-5100.2005.tb00140.x.

Roberts, M.P., and Finger, F., 1997, Do U-Pb zircon ages from granulites reflect peak metamorphic conditions?: Geology, v. 25, p. 319–322, https://doi.org/10.1130/0091-7613(1997)025<0319:DUPZAF>2.3.CO;2.

Rosenberg, C.L., and Handy, M.R., 2005, Experimental deformation of partially melted granite revisited: Implications for the continental crust: Journal of Metamorphic Geology, v. 23, p. 19–28, https://doi.org/10.1111/j.1525-1314.2005.00555.x.

Rubatto, D., and Hermann, J., 2003, Zircon formation during fluid circulation in eclogites (Monviso, Western Alps): Implications for Zr and Hf budget in subduction zones: Geochimica et Cosmochimica Acta, v. 67, p. 2173–2187, https://doi.org/10.1016/S0016-7037(02)01321-2.

Rubatto, D., and Hermann, J., 2007, Zircon behaviour in deeply subducted rocks: Elements, v. 3, p. 31–35, https://doi.org/10.2113/gselements.3.1.31.

Sorensen, S.S., Grossman, J.N., and Perfit, M.R., 1997, Phengite-hosted LILE enrichment in eclogite and related rocks: Implications for fluid-mediated mass transfer in subduction zones and arc magma genesis: Journal of Petrology, v. 38, p. 3–34, https://doi.org/10.1093/petroj/38.1.3.

Thomson, O.A., Cavosie, A.J., Moser, D.E., Barker, I., Radovan, H.A., and French, B.M., 2014, Preservation of detrital shocked minerals derived from the 1.85 Ga Sudbury impact structure in modern alluvium and Holocene glacial deposits: Geological Society of America Bulletin, v. 126, p. 720–737, https://doi.org/10.1130/B30958.1.

Watson, E.B., and Harrison, T.M., 1983, Zircon saturation revisited temperature and composition effects in a variety of crustal magma types: Earth and Planetary Science Letters, v. 64, p. 295–304, https://doi.org/10.1016/0012-821X(83)90211-X.

Manuscript received 7 August 2017
Revised manuscript received 20 November 2017
Manuscript accepted 21 November 2017

Printed in USA